Journal of Sound and Vibration 331 (2012) 4609–4628

Contents lists available at SciVerse ScienceDirect

Journal of Sound and Vibration

journal homepage: www.elsevier.com/locate/jsvi

Review

Aeroacoustics research in Europe: The CEAS-ASC report on 2011 highlights

A. McAlpine *, R.J. Astley

Institute of Sound and Vibration Research, University of Southampton, Highfield, Southampton SO17 1BJ, UK

ARTICLE INFO

Article history:
Received 26 April 2012
Accepted 8 May 2012
Handling Editor: P. Joseph
Available online 22 June 2012

ABSTRACT

The Council of European Aerospace Societies (CEAS) Aeroacoustics Specialists Committee (ASC) supports and promotes the interests of the scientific and industrial aeroacoustics community on an European scale and European aeronautics activities internationally. In this context, "aeroacoustics" encompasses all aerospace acoustics and related areas. Each year the committee highlights some of the research and development projects in Europe.

This paper is a report on highlights of aeroacoustics research in Europe in 2011, compiled from information provided to the ASC of the CEAS.

During 2011, a number of research programmes involving aeroacoustics were funded by the European Commission. Some of the highlights from these programmes are summarized in this paper, as well as highlights from other programmes funded by national programmes or by industry. Furthermore, a concise summary of the CEAS-ASC workshop "Acoustic Liners and Associated Propagation Techniques" held in Lausanne in October 2011 is included in this report.

Enquiries concerning all contributions should be addressed to the authors who are given at the end of each subsection.

Contents

1. CEAS-ASC workshop . . . 4610
2. Airframe noise . . . 4610
   2.1. Aeroacoustic investigation of a high-lift device by means of simultaneous PIV and microphone array measurements . . . 4610
3. Fan and Jet noise . . . 4611
   3.1. Jet flow aeroacoustics at $Re=93{,}000$: comparison between experimental results and numerical predictions . . . 4611
   3.2. Instability waves and large-scale mixing noise in subsonic coaxial jets . . . 4612
   3.3. Reformulation of acoustic entropy source terms . . . 4613
   3.4. Azimuthal-modal approach for jet mixing noise using hybrid RANS/CAA method . . . 4613
4. Propeller noise . . . 4614
   4.1. Prediction of near- and far-field noise generated by contra-rotating open rotors . . . 4614
   4.2. Aeroacoustic computations of a contra-rotating open rotor model accounting for test rig installation effects . . . 4615
5. Techniques and methods in aeroacoustics . . . 4616
   5.1. Extension of Amiet's theory for the aeroacoustic analysis of a wing-flap configuration including acoustic scattering . . . 4616
   5.2. Integrated CFD-aeroacoustic simulations . . . 4616

* Corresponding author. Tel.: +44 23 8059 2667; fax: +44 23 8059 3190.
E-mail addresses: am@isvr.soton.ac.uk (A. McAlpine), rja@isvr.soton.ac.uk (R.J. Astley).

0022-460X/$ - see front matter © 2012 Elsevier Ltd. All rights reserved.
http://dx.doi.org/10.1016/j.jsv.2012.05.012

5.3. Optical acoustic pressure measurements in a large-scale test facility with mean flow 4617
5.4. Microphone array measurements under combined pressurized cryogenic conditions 4617
5.5. 2-D evaluation of turbulent boundary layer pressure fluctuations at cruise flight condition 4618
5.6. Slowly varying modes in an APU exhaust duct 4619
5.7. Acoustic modes in a duct containing a parabolic shear flow 4620
5.8. On sound generation by moving surfaces and convected sources in a flow 4621
5.9. Experimental source characterization techniques for studying the acoustic properties of perforates under high level acoustic excitation. 4621
5.10. Simulations of duct acoustics with the frequency-domain linearized Navier–Stokes equations 4621
5.11. Efficient parallel computing with high-order compact schemes for aeroacoustic simulations 4623
6. Miscellaneous topics 4623
6.1. Uncertainty quantification for the trailing-edge noise of a controlled-diffusion airfoil 4623
6.2. Acoustic characterization of orifices under grazing flow 4624
6.3. Aircraft noise modelling and assessment in IESTA 4624
6.4. CFD–CAA coupled calculations of a tandem cylinder configuration to assess facility installation effects 4625
6.5. Aeroacoustic investigations of a generic fan-in-wing configuration 4626
References 4627

1. CEAS-ASC workshop

The fifteenth CEAS-ASC workshop on ‘‘Acoustic Liners and Associated Propagation Techniques” was held at the École Polytechnique Fédérale de Lausanne (EPFL), Switzerland, on October 13–14, 2011. It was the fifth workshop sponsored by the Aeroacoustics Committee of the AIAA, and also the first scientific workshop to be sponsored by the X-Noise EV Coordination and Support Action project of the 7th Framework Program of the European Commission. The workshop was locally organized by Hervé Lissek, Pénélope Leyland and Cécile Deslot (EPFL). Eighty participants from 21 countries (from Europe, North America and Japan) attended the event, mainly coming from the aerospace industry and research institutions.

Acoustic liners are key aircraft components for the reduction of engine noise. Although existing liners' design architectures already achieve significant noise reductions, there is still work to be done to improve attenuation performance, with a view to achieving the objectives of the ACARE (Advisory Council for Aeronautics Research in Europe) visions for 2020, and beyond, towards 2050. The many on-going research efforts on acoustic liners, such as those reported during this workshop, provide a clear illustration of the importance of the subject.

There were 27 papers presented at the Lausanne workshop. These were categorized in the following sub-topics: novel lining concepts (active, passive or adaptive), measurement techniques for the assessment of liner performance, methods for predicting liner impedance (experimental, numerical and analytical), methods for predicting far-field propagation, design optimization with a view to lowering community and/or interior noise, and a focus on two specific national research initiatives oriented towards liner improvement. Three keynote speakers structured this framework of presentations. Andrew Kempton, Rolls–Royce plc, UK, outlined the state of the art on acoustic liners, and presented the general requirements specifying the design of acoustic liners, and also experimental methods for assessing such performances, in his talk ‘‘Acoustic liners for modern aero-engines”. Daniel Bodony, University of Illinois, USA, presented a liner eduction methodology using large-eddy and direct numerical simulations in his talk ‘‘Direct numerical simulation of acoustic liners: results and time-domain modelling”. Finally, Jean-Pierre Coyette, Free Field Technology, Belgium, presented the issues, and solutions, for modelling acoustic propagation with flow in ducts, in his talk ‘‘Computational tools for modelling acoustic liners and propagation: review of some key ingredients and challenges”. Owing to the large number of contributions, no final round table was organized.

Written by H. Lissek: herve.lissek@epfl.ch, École Polytechnique Fédérale de Lausanne, Switzerland.

2. Airframe noise

2.1. Aeroacoustic investigation of a high-lift device by means of simultaneous PIV and microphone array measurements

The noise sources at the leading edge slat in the DLR (German Aerospace Centre) F16 high-lift device configuration have been investigated by means of the causality correlation method [1]. The model chord length is $c=300$ mm (clean configuration) and the span measures 800 mm. The cross-correlation between the acoustic far-field pressure and near-field fluctuations obtained via particle image velocimetry (PIV) was calculated. A parametric study was performed varying the deflection-angle α, the slat-gap and -overlap as well as the flow speed U_∞. In the case of shallow deflection-angles the temporal evolution of the correlation $R_{v,p}$ between the far-field pressure p and the vertical velocity component v shows a strong periodicity (Fig. 1, τ is the retarded time). This temporal evolution together with the spatial distribution of the coefficient corresponds to a regular pattern of discrete vortices emanating from the slat cusp and being accelerated and ejected through the slat gap (Fig. 2). Thus these coherent structures can be identified as part of the sound generation process [2]. For higher deflection angles very similar flow structures are present in the slat-cove region. But here only a comparatively small region of significant correlation values can be identified. This corresponding single positive and

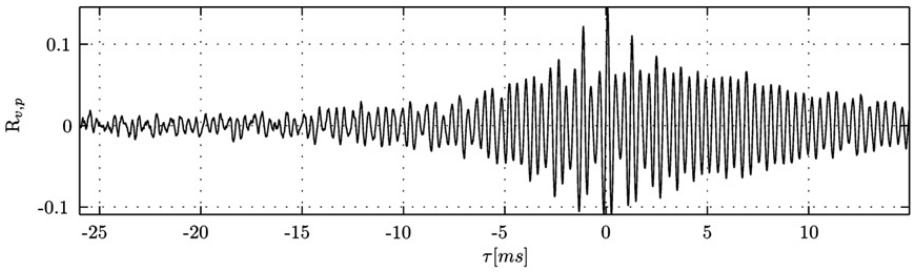

Fig. 1. Case $\alpha = 11^\circ$ at $U_\infty = 50$ m s^{-1}. Temporal evolution of the cross-correlation coefficients $R_{v,p}$ at position $[x/c,y/c] = [0.058,0.032]$ where the overall maximum of the correlation coefficient is located.

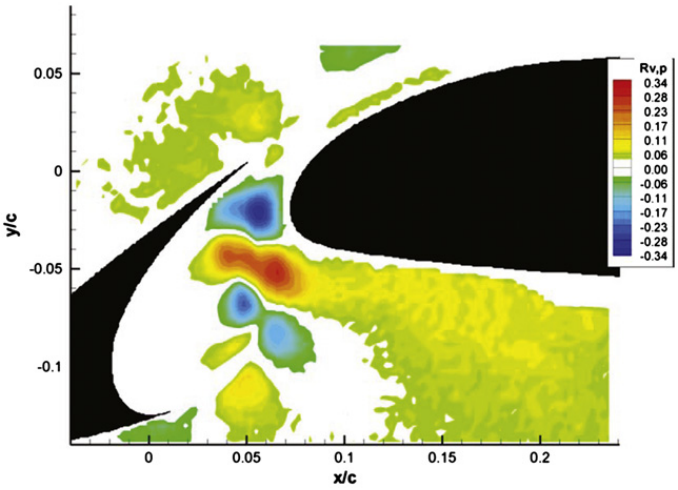

Fig. 2. Case $\alpha = 11^\circ$ at $U_\infty = 50$ m s^{-1}. Instantaneous distribution of the cross-correlation coefficient $R_{v,p}$ for $\tau = 0$ ms.

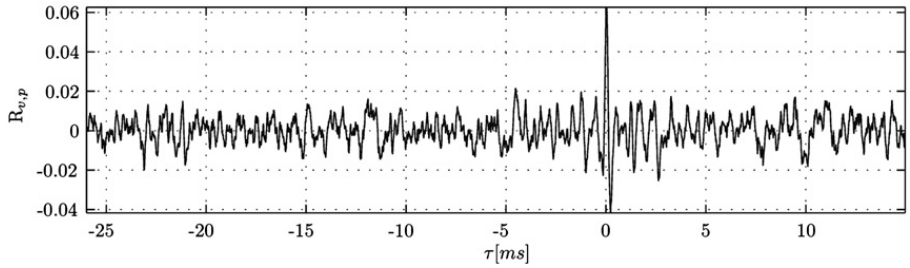

Fig. 3. Case $\alpha = 15.5^\circ$ at $U_\infty = 50$ m s^{-1}. Temporal evolution of the cross-correlation coefficients $R_{v,p}$ at position $[x/c,y/c] = [0.052,-0.024]$ where the overall maximum of the correlation coefficient is located.

negative deflection in the temporal evolution of the correlation function (Fig. 3) is typical for a source process with a broadband characteristic [3]. The results show that a parameter change can be directly assigned to different flow structures which are part of the sound generation process by means of the proposed causality correlation method.

Written by A. Henning: arne.henning@dlr.de, DLR, Germany.

3. Fan and Jet noise

3.1. Jet flow aeroacoustics at Re=93,000: comparison between experimental results and numerical predictions

This work concerns the numerical prediction of noise from a subsonic jet at a relatively high Reynolds number: $Re = UD/\nu = 93,000$, where U is the jet velocity, ν is the kinematic viscosity and $D = 2R$ is the diameter of the nozzle [4]. The simulated flow corresponds to the experiment performed by Schram et al. [5]. This experiment consisted of a low Mach number excited jet, and was measured using particle image velocimetry (PIV). The pairing of vortex rings is one of the basic mechanisms for sound production in subsonic free jets. Based on the description of the experiment, simulations of two axisymmetric flow configurations were considered: (1) the DNS (direct numerical simulation) of the pairing of an isolated vortex pair using, as initial condition, a PIV field extracted from the experimental jet; (2) the DNS of the jet with

the same physical parameters as those of the experiment (Fig. 4). The acoustic source terms were evaluated using vorticity-based analogies (see [5]) for the two simulations, and compared to those evaluated from the experiment. This study is a continuation of the work of Detandt et al. [6], who performed the comparison at a moderate Reynolds number $Re=14{,}000$. The results obtained for the isolated pairing show some discrepancies with the experimental jet results, whereas the jet simulation is in very good agreement with the experiment (Fig. 4), provided a proper reduction technique is used to isolate the merging vortex rings from the rest of the jet.

Written by L. Bricteux: laurent.bricteux@umons.ac.be, M. Duponcheel and G. Winckelmans, Université Catholique de Louvain, Belgium, and C. Schram, von Karman Institute, Belgium.

3.2. Instability waves and large-scale mixing noise in subsonic coaxial jets

The precise role of large-scale structures in jet noise generation mechanisms is still not completely understood. A popular approach to gain insight into the physics of jets, and to predict the associated acoustic fields, lies in large eddy simulation (LES) methods. Despite increasingly favorable comparisons with far-field acoustic measurements, such an approach hardly reveals to what extent instability waves contribute to jet noise. A more subtle approach, based on parabolized stability equations (PSE), and focusing on the axial evolution of selected unstable modes, has been employed in the past decade in order to better assess the exact hydrodynamic and acoustic role of these coherent structures in subsonic and supersonic jets.

Such a PSE analysis has been extended to the complex industrial case of subsonic coaxial jets. In particular, based on a large data set acquired in the framework of the EU collaborative research project CoJeN, linear PSE computations were performed in order to study the hydrodynamic features of both the inner and outer mixing layers. Growth and decay of the resulting wave-packets was revealed to be an efficient noise generator mechanism even in subsonic jets. Indeed, even though the PSE method is inherently not able to accurately capture the acoustic radiation of spatially modulated wavepackets, a Kirchhoff-type technique allows the acoustic field to be reconstructed as shown in Fig. 5(a). The resulting noise radiation in the far-field compares very favorably, at low angles, with corresponding measurements over the entire frequency range where the maximum sound pressure levels are observed, as shown in Fig. 5(b). Moreover, a finer analysis

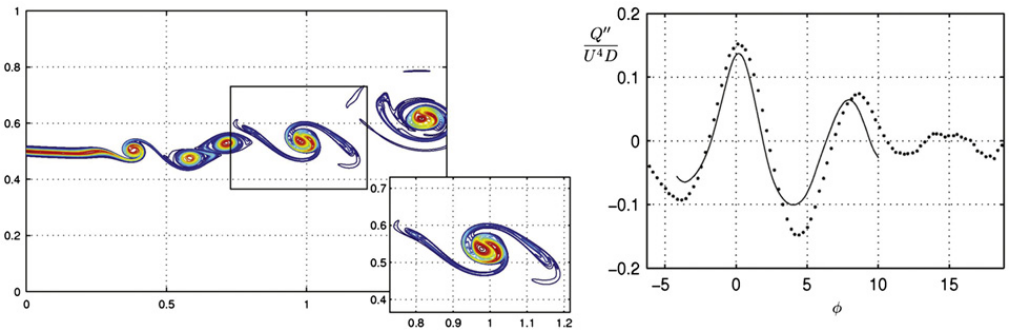

Fig. 4. Snapshot of the vorticity field for the jet with moving integration window (left). The effect of the improved eduction technique is illustrated in the lower window where the unwanted vorticity features are discarded. Acoustic source term for the conservative analogy [5] (right): experimental results (bullets), DNS of the jet with improved post-processing (solid line).

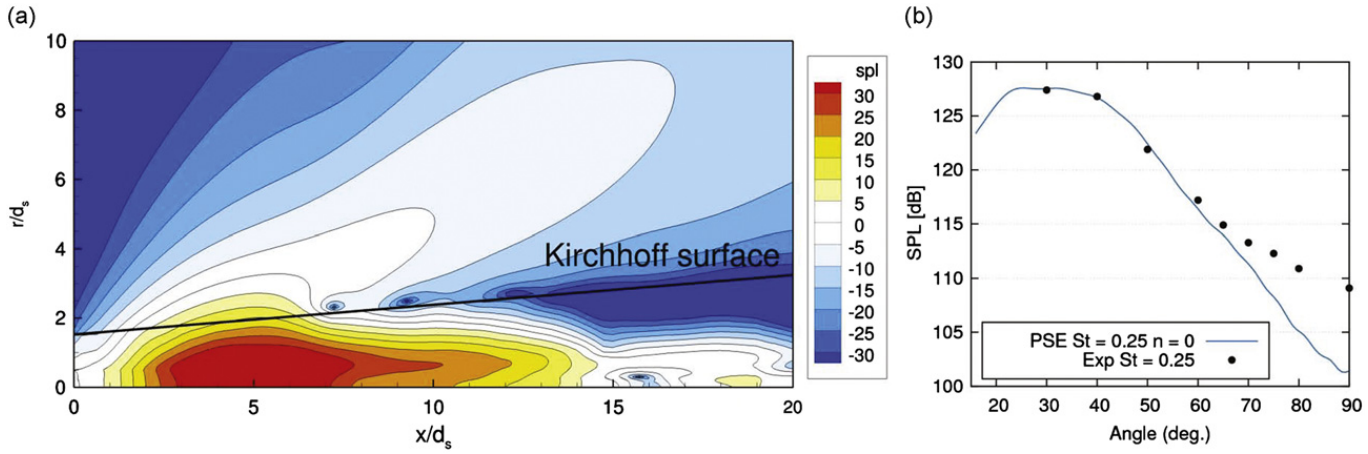

Fig. 5. Acoustic propagation of the linear PSE pressure field computed on a coaxial jet for the axisymmetric mode and $St=0.25$: (a) near field, (b) far field with comparison against measurements.

of the measured near-field pressure showed characteristic signatures of the computed PSE modes, supporting the conclusions of the analysis.

Written by O. Léon: olivier.leon@onera.fr, and J-P. Brazier, ONERA, France.

3.3. Reformulation of acoustic entropy source terms

Non-uniform density distributions play an important role in the propagation of sound, for instance, in a flow with a pronounced temperature gradient. The sound mechanism contains additional sources in the unsteady density field, i.e., the acoustic radiation from a sheared mean flow is amplified by scattering from the mean density gradient. However, the identification of real sources in realistic turbulent flows is hard to achieve since the sound generation is only a small fraction of the energy of the entire fluid dynamic process. Recently, a source reformulation was presented based on the acoustic perturbation equations (APE) which is valid for a wide class of configurations [7,8]. The entropy source term in the original APE formulation inherently includes low-order, i.e., linearized, sound sources which can easily overestimate the low frequency sound. That is, the expression of the original formulation increases the acoustic power due to the linearization of the second law of thermodynamics. The physical reason for the over-prediction of the sideline acoustics in the high frequency band is the absence of the source cancellation of the small-scale turbulence. The proposed new entropy term based on the excess density does not introduce this surplus sound (Fig. 6).

Written by S. Koh: s.koh@aia.rwth-aachen.de, G. Geiser and W. Schröder, RWTH Aachen University, Germany.

3.4. Azimuthal-modal approach for jet mixing noise using hybrid RANS/CAA method

In the framework of the project OPTITHECK in collaboration with Rolls-Royce Deutschland, an efficient methodology to predict broadband fine-scale jet noise has been approved and verified. For this kind of jet noise computations the precomputed CFD-data (RANS) can be used to gain the statistical quantities such as turbulence kinetic energy, time and length scales, which are used to model the acoustic sources, realized by the random particle method (RPM). The acoustic source model, based on the formulation of Tam and Auriault [9] is applied to RPM [10]. The acoustic fluctuations are generated as a 4-D synthetic turbulent pressure, which are then propagated by means of state-of-the-art CAA tools.

For the commonly used isolated configurations of jet nozzles, the advantage of axi-symmetry can be exploited. To take this into account, by means of Fourier series decomposition in azimuthal direction, a 3-D jet noise problem can be decomposed into several 2-D problems [11,12], which means a drastic reduction of computational effort if the number of azimuthal modes remains small. Nevertheless, all 3-D physical effects are captured.

The results have shown that with only six modes, very accurate predictions of jet noise can be made up to a Strouhal number of about 10 (Fig. 7). Especially, the contribution of individual azimuthal mode spectra to the overall spectrum show interesting behavior. From these results, there is a frequency range for each azimuthal mode where its contribution to the sound pressure levels is crucial. The investigation of the Mach scaling in the range $M_a=0.3$–0.9 has shown that the computational results match well with the genuine model of Tam and Auriault and with measurements. With the empirically adjusted constants of Tam and Auriault, absolute prediction of sound pressure levels is possible (Fig. 8).

Written by A. Neifeld: andrej.neifeld@dlr.de and R. Ewert, DLR, Germany.

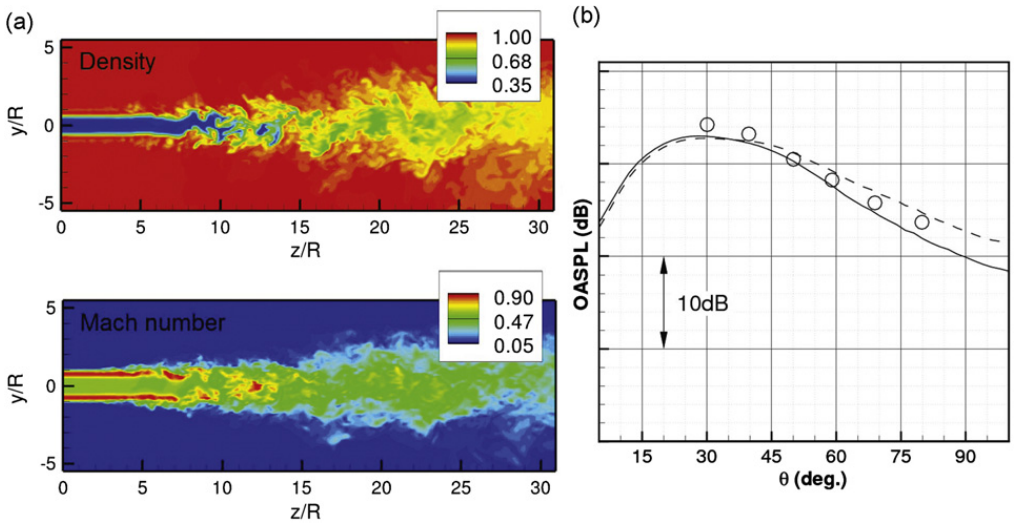

Fig. 6. Coaxial jet possessing a helium-mixture core flow: (a) density and Mach number contours, (b) overall sound pressure level determined by the reformulated sources (solid line) and the old source formulation (dashed line). The open circles denote the experimental data provided by C.J. Mead, QinetiQ Ltd (Mead, C.J., CoJeN deliverable 0.1, Sixth Framework Programme EC Contract No. AST3-CT-2003-502790, 2004).

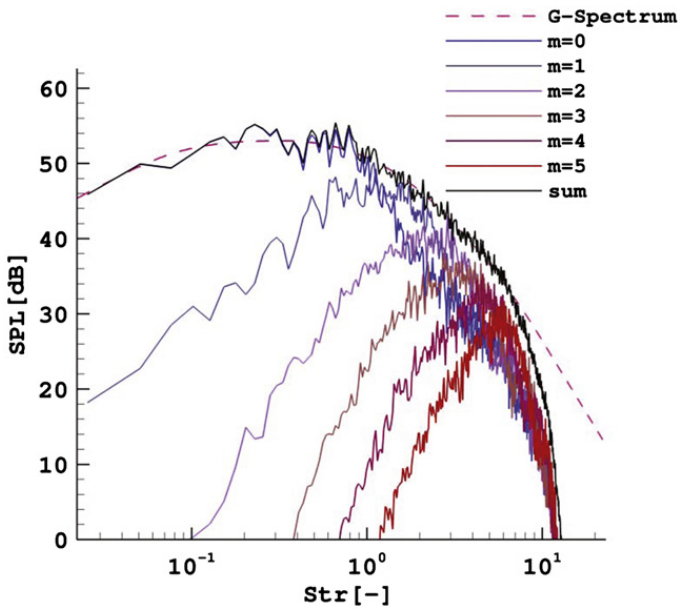

Fig. 7. Comparison between the fine-scale noise similarity spectra (G-Spectrum) and individually numerically computed azimuthal modes ($m=0\ldots5$) for the EU-JEAN nozzle, which are summed up to a single spectrum; cold single stream jet with $M_a=0.3$ at $\theta=90^\circ$ at jet axis distance $R/D=10$.

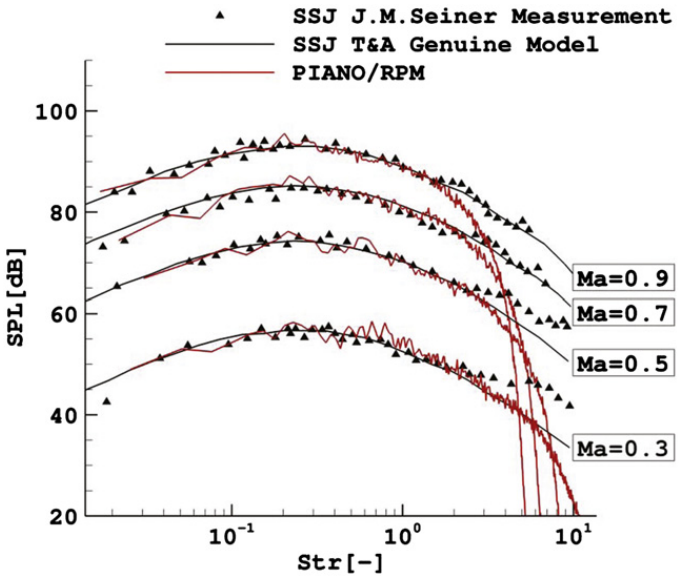

Fig. 8. Comparison between the fine-scale noise spectra predictions of Tam and Auriault, the measurements and numerically computed sum spectra for Mach numbers $M_a=0.3,0.5,0.7,0.9$; cold single stream jet with $M_a=0.3$ at $\theta=90^\circ$ at jet axis distance $R/D=10$.

4. Propeller noise

4.1. Prediction of near- and far-field noise generated by contra-rotating open rotors

Contra-rotating open rotors (CROR) are receiving renewed interest by airplane and engine manufacturers due to their great potential for fuel savings. NUMECA Int. has developed an innovative aeroacoustic prediction method for CRORs based on the nonlinear harmonic method (NLH) for the CFD computations, and on the Ffowcs Williams and Hawkings (FW-H) equations for the far-field acoustic propagation. This method has since been tested on numerous take-off and cruise configurations. The NLH method has proven to be a very cost efficient, and an accurate alternative to full unsteady simulations for CROR configurations, allowing a gain of several orders of magnitude in terms of CPU needs. The proposed aerodynamic and acoustic methodology has largely been validated against other numerical codes. During the course of the EU Clean Sky project DINNO-CROR, a sensitivity analysis on certain numerical parameters has been performed, to provide guidelines for the numerical prediction of CROR noise. Among others, the influence of the type of FW-H surface and the

number of harmonics on the accuracy of the results has been studied, along with a grid refinement analysis. Numerical results are currently being compared to experimental data in the framework of the EU Clean Sky project NAA-CROR to further validate the numerical methodology [13].

Written by T. Deconinck: thomas.deconinck@numeca.be, A. Capron and C. Hirsch, Numeca International, Belgium.

4.2. Aeroacoustic computations of a contra-rotating open rotor model accounting for test rig installation effects

Within the framework of the European project DREAM, ONERA (The French Aerospace Lab.) has performed aerodynamics and aeroacoustics computations of a contra-rotating open rotor model that has been tested in the T-104 wind tunnel at TsAGI, Russia. This test rig exhibits strong aerodynamic installation effects that had to be taken into account in the computations to be consistent with the experiments. Based on the geometry provided by TsAGI, the test rig has been simplified and meshed. URANS computations of the test rig with a contra-rotating open rotor model (200 million cells) have been carried out using the elsA CFD solver using Chimera grids to account for rotating parts and struts (Fig. 9). Aeroacoustic computations have been performed using the solid surface formulation of the Ffowcs Williams and Hawking equation solved by the KIM code. Two sets of acoustic computations have been carried out, the first one using rotor blade pressures and rotating hubs wall pressures as input data, the second one using the full test rig (including the open rotors) wall pressures as input data. The directivities computed at experimental microphone locations show that using the full rig wall pressures for the acoustic computations is required to match the measured directivities (Fig. 10).

Written by F. Falissard: fabrice.falissard@onera.fr, R. Boisard and G. Delattre, ONERA, France.

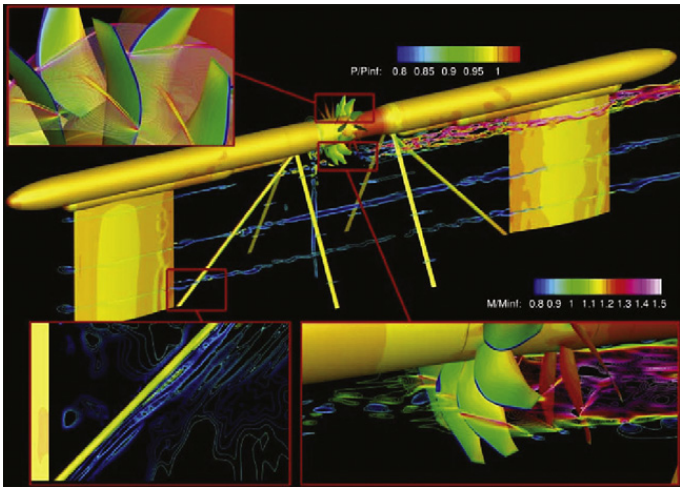

Fig. 9. Aerodynamic flowfield around TsAGI test rig with contra-rotating open rotor.

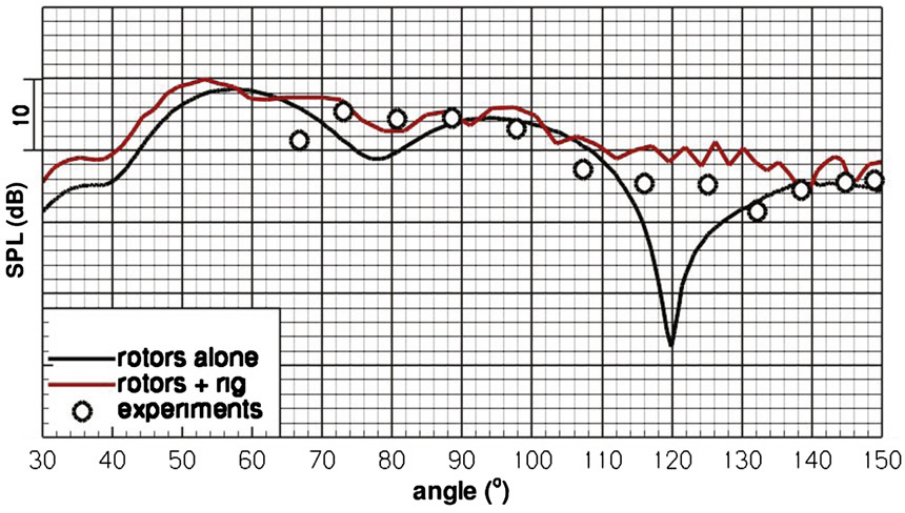

Fig. 10. First interaction tone directivity computed using rotor blade pressures only and rotor blade and test rig wall pressure.

5. Techniques and methods in aeroacoustics

5.1. Extension of Amiet's theory for the aeroacoustic analysis of a wing-flap configuration including acoustic scattering

In order to study the noise generated by a wing-flap configuration, KU Leuven combined Amiet's theory with a boundary element method (BEM). The installation and sound scattering effects of the wing-flap configuration are studied using BEM. The flap is modelled as a noise source, represented by a series of discrete dipoles, whose strength is defined by Sears' or Amiet's theory, and the wing is considered as a rigid scattering surface. The calculated directivity (Fig. 11) is compared to the free-field directivity and the differences are explained by the different impedance and the compactness effects of the wing and the flap. The aerodynamic noise generation of the wing-flap configuration is studied using an extension of Amiet's trailing edge noise theory. The adopted approach is based on a broadband extension of Amiet's trailing edge noise model [14], which extends the validity to the geometrical near-field and introduces the acoustic scattering. The wall-pressure spectrum, needed as input for this model, is reconstructed from RANS data [15], and the spanwise correlation length is modelled using Corcos' model. A comparison with experimental data shows that this approach correctly reproduces the order of magnitude of the power spectral density of the far-field acoustic pressure (Fig. 12). The differences between the spectrum of the acoustic pressure generated by the wing in free-field, and in the presence of the flap, are shown to be mainly caused by the noise generated by the flap, whilst the scattering of the sound waves has a negligible influence for the specified observer position [16].

Written by H. Denayer: herve.denayer@mech.kuleuven.be, W. De Roeck and W. Desmet, Katholieke Universiteit Leuven, Belgium.

5.2. Integrated CFD-aeroacoustic simulations

In the last year, NUMECA has developed a unique integrated simulation platform for aeroacoustic applications that naturally integrates noise propagation tools, noise characterization tools, and CFD analysis in a single software

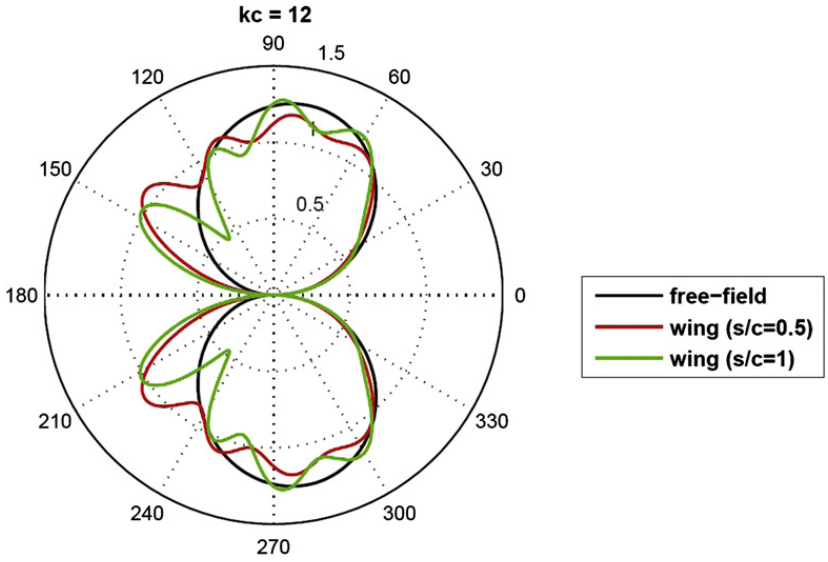

Fig. 11. Comparison of the directivity pattern at 5 m between the free-field solution and the BEM solution, including acoustic scattering.

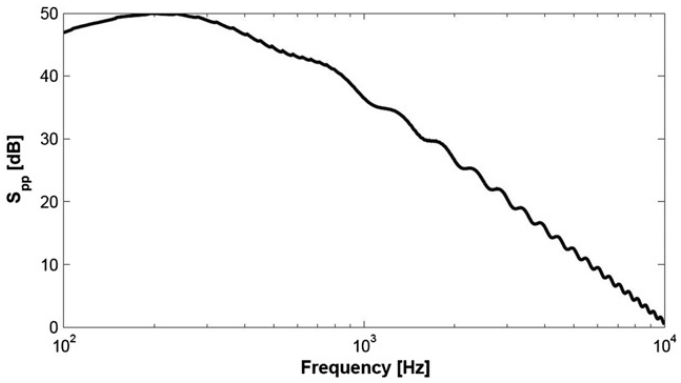

Fig. 12. Power spectral density at 2 m and 85° from the wing trailing edge of the noise generated by the wing-flap configuration.

environment. It allows integrated aeroacoustic simulations for several demanding application domains including, for example, nacelle noise, high-lift device noise, fan noise, and many others.

The platform is based on an advanced BEM–FEM noise propagation tool (VNoise) that is fully integrated with the NUMECA CFD solvers FINE/Open and FINE/Turbo. In particular the possibility to directly couple with FINE/Turbo NLH solver can reduce computational times for tone noise predictions by several orders of magnitude.

The platform also includes a specific module dedicated to the stochastic reconstruction of flow turbulence starting from a simple RANS analysis. The approach is based on the coupling of an enhanced SNGR approach with a multi-domain propagation technique that ensures maximum flexibility in different application contexts [17], and can be considered as a simplified approach that enables, when aerodynamics and aeroacoustics are not strongly coupled, with engineering approximations the evaluation of broadband noise radiated by turbulent flows.

Written by P. di Francescantonio: pdifra@sts-web.it, Software Tecnico Scientifico, Italy.

5.3. Optical acoustic pressure measurements in a large-scale test facility with mean flow

A non-intrusive technique of acoustic pressure measurements within a wind tunnel has been tested in the ONERA (The French Aerospace Lab.) F2 facility [18]. A three-components laser doppler anemometer (LDA) has been used to measure the velocity field in the vicinity of a nose-coned benchmark microphone. A flow velocity of 40 m s^{-1} was imposed within the test section and an acoustic signal made of 11 pure tones between 300 and 3000 Hz was emitted by a loudspeaker located in the floor. A post-processing technique based on cross-correlations with the loudspeaker signal allows reducing the acoustic component from the velocity field. The acoustic velocity is measured on a 64 points cube of side length 12.5 mm, and its spatial gradients are computed by finite differences. Then, the associated LDA acoustic pressure is computed from the linearized Euler equations. This whole process has been applied for two measurement positions within the test section. In both cases, the comparison between the sound pressure levels obtained by LDA and those measured by the benchmark microphone are quite satisfactory, except for the lowest frequency where the sound pressure levels are over-estimated by the LDA method, which is probably due to the effect of phase errors on the velocity differentiation (Fig. 13). It has been shown that the accuracy of the LDA acoustic pressure assessment can be improved by increasing the number of measurements and by taking their mean value. These developments are the subject of a patent (INPI No. FR-2951276/15 avril 2011).

Written by E. Piot: estelle.piot@onera.fr, F. Micheli and F. Simon, ONERA, France.

5.4. Microphone array measurements under combined pressurized cryogenic conditions

The microphone array measurement technique for cryogenic application down to 100 K has been developed and successfully applied to a high-lift configuration [19,20]. To achieve real-flight Reynolds numbers, an additional increase of the static pressure is needed. The European Transonic Windtunnel GmbH (ETW) can provide real-flight Reynolds numbers by virtue of both decreased temperature and increased pressure. For the development of the measurement technique, aeroacoustic tests were conducted at the Pilot-ETW, a small scale wind tunnel used for preliminary testing [21].

Brüel and Kjær cryogenic condenser microphones of type 4944A were used. Preliminary sensor tests have been performed to obtain the frequency response at different static pressures and different temperatures. The resulting amplitude response was shown not to be a linear combination of the amplitude response caused by varying the static pressure or temperature separately.

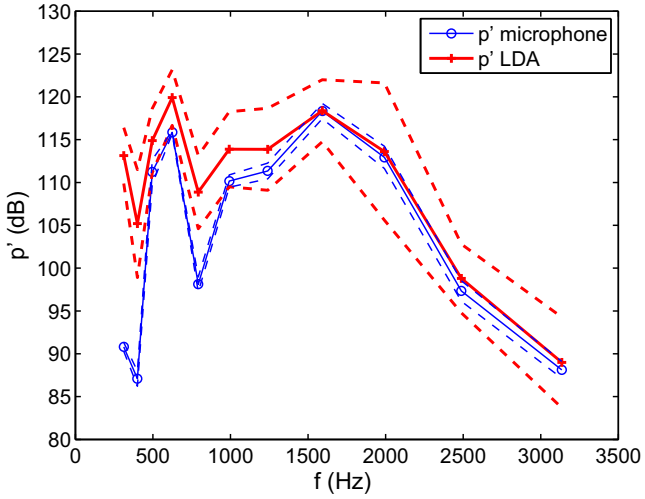

Fig. 13. Comparison of sound pressure level (dB) obtained by LDA and by microphone.

Using these sensors, a microphone array suitable for cryogenic and pressurized testing consisting of 12 microphones has been designed. Measurements have been performed in the Pilot-ETW for various Reynolds numbers using a cylinder of 2 mm diameter as an aeroacoustic source. Condition corrections were applied for temperature and pressure. Fig. 14 shows the focused sound pressure levels for different static pressures at ambient temperature (top) and at a temperature of 120 K (bottom). For Reynolds number up to 75×10^3 only small differences can be seen. A further increase of the Reynolds number leads to a diminishing peak height at the vortex shedding frequency, caused by the first onset of transition in the free sheer layers of the cylinder wake.

Written by T. Ahlefeldt: thomas.ahlefeldt@dlr.de, DLR, Germany.

5.5. 2-D evaluation of turbulent boundary layer pressure fluctuations at cruise flight condition

Spatial coherence of turbulent boundary layer pressure fluctuations has been investigated on an Airbus model A320 aircraft at a Mach number of $M=0.78$ and flight altitude of 10,668 m (FL 350) [22,23]. The coherence lengths of turbulent structures are extracted both parallel and perpendicular to the flow direction at three dummy windows located approximately 1 m in front of the wing. Using an irregularly shaped pressure transducer array, the maximum coherence length is extracted (Fig. 15) and implies a flow direction different from the fuselage angle-of-attack. The local flow direction changes with variation of the adopted frequency for the coherence analysis. This is believed to be caused by the wing-induced pressure gradient on the flow. It causes vortex structures of different sizes and frequencies at the wall to be transported in different directions within the

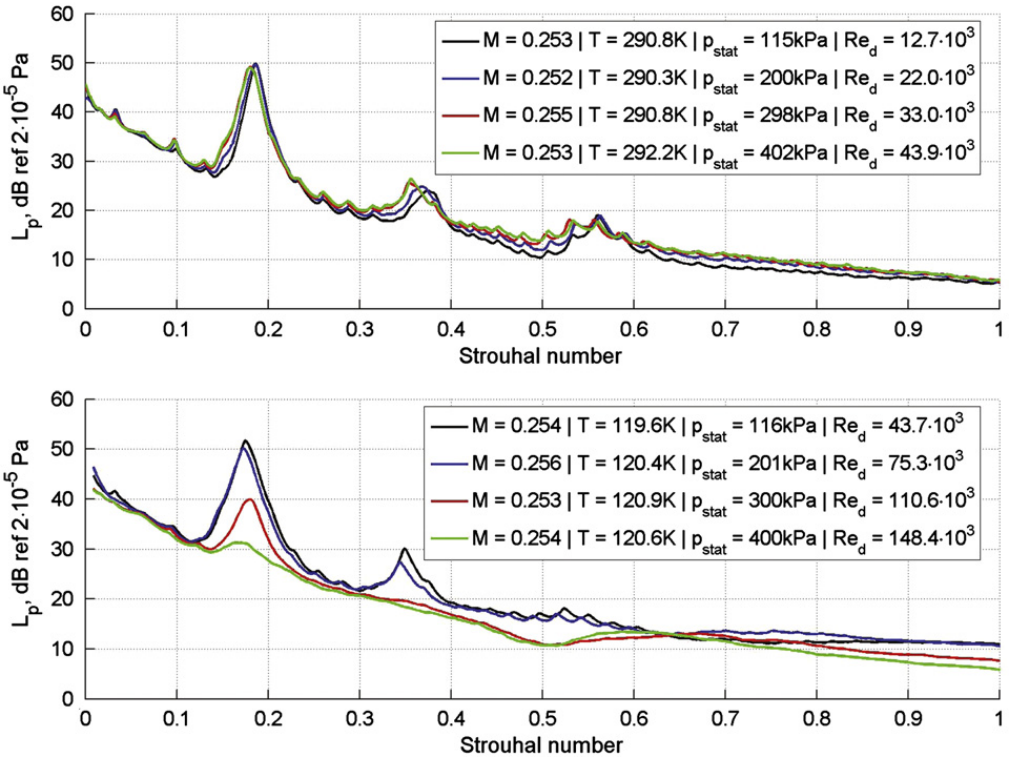

Fig. 14. Sound pressure level versus frequency normalized with freestream velocity and cylinder diameter (Strouhal number) for several static pressures at a Mach number of $M=0.25$. The temperature is $T=290$ K (top) and $T=120$ K (bottom), leading to a different Reynolds number range.

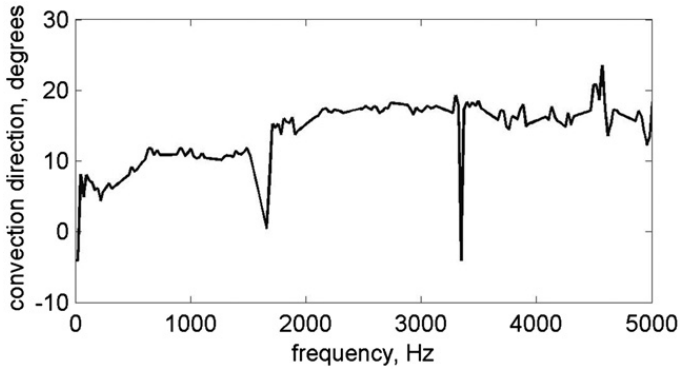

Fig. 15. Angle of maximum coherence length.

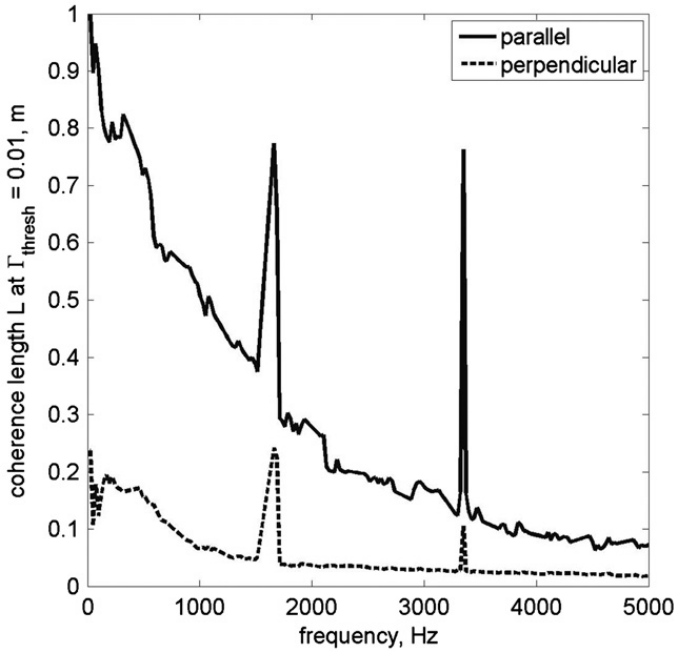

Fig. 16. Coherence length extracted from flight test data.

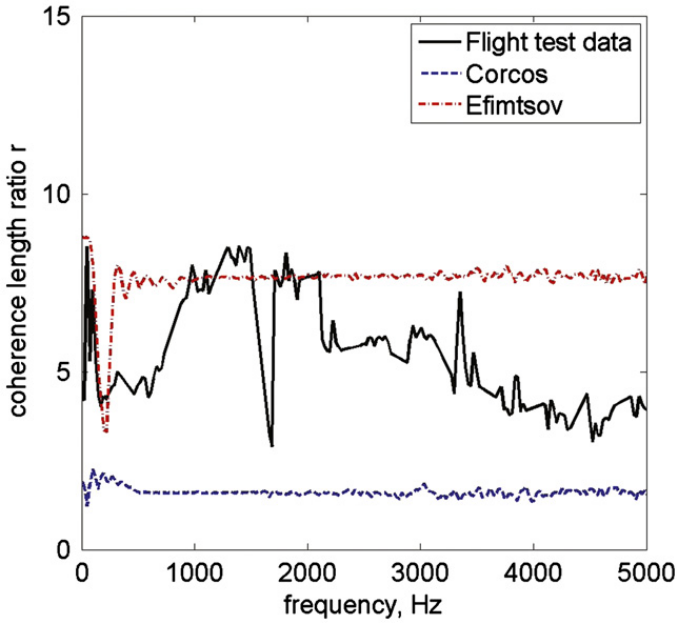

Fig. 17. Ratio of longitudinal to lateral coherence.

boundary layer. Fig. 16 shows the extracted coherence lengths, when flow direction is taken into account. Displayed in the figure are the distances after which a coherence of 1% is still present between two transducer signals. A longer coherence in the flow direction due to convection is clearly visible in the graph. Two peaks at 1600 and 3200 Hz coincide with the blade passage frequency of the jet engine fan. A dependency on the frequency is also observed in the ratio of longitudinal to lateral coherence lengths (Fig. 17). The measured data lies between the values predicted by the models of Corcos [24] and Efimtsov [25]. For this comparison, an in-flight boundary layer thickness was taken from similar flight measurements [26].

Written by S. Haxter: stefan.haxter@dlr.de and C. Spehr, DLR, Germany.

5.6. *Slowly varying modes in an APU exhaust duct*

Reduction of auxiliary power unit (APU) noise may be achieved by liners in the exhaust duct, which is typically straight with an axially varying liner depth, a non-uniform mean flow and strong temperature gradients. An analytically explicit

solution is obtained in the form of slowly varying modes of WKB-type for the acoustic field inside a duct with an impedance that is continuously varying in the axial direction (Fig. 18). In the cross-wise direction each WKB-mode is given by eigenfunction-type solutions of the Pridmore–Brown equation. These solutions are obtained by a collocation method supplemented by a path-following procedure [27].

Written by S. Rienstra: s.w.rienstra@tue.nl, Eindhoven University of Technology, The Netherlands.

5.7. Acoustic modes in a duct containing a parabolic shear flow

The acoustics of shear flows is relevant to sound transmission in shear layers and boundary layers, including those associated with engine nozzles and inlets. The acoustic wave equation in an unidirectional shear flow is known as the Pridmore–Brown (1958) or Lilley (1973) equation although it dates further back to Haurwitz (1934). Four exact solutions have been published, for a linear velocity profile homentropic [28] or homenergetic [29] and exponential [30] and hyperbolic tangent [31] velocity profiles. A fifth exact solution has been obtained for a parabolic velocity profile, relevant to the acoustics of ducted flows [32]. It applies to upstream or downstream propagation in subsonic or supersonic flows. In the case of upstream propagation in a supersonic flow there are critical layers where the flow velocity equals the sound speed. These are singularities of the wave equation and correspond to energy exchange between the sound and mean flow, e.g. attenuation, amplification, reflection or mode conversion. It is shown that the critical layers separate regions of the flow with distinct eigenvalues and eigenfunctions (Fig. 19). Thus for upstream propagation in a supersonic shear flow in a duct there is no single system of acoustic modes valid across the duct: there are distinct sets of acoustic modes separated by the critical layers, as if these were 'fluid walls'. The eigenvalues or natural frequencies and eigenfunctions or acoustic modes have been obtained for all cases of downstream or upstream propagation, the latter with and without critical layers. Also rigid and impedance wall boundary conditions have been considered.

Written by L.M.B.C. Campos: luis.campos@ist.utl.pt, Instituto Superior Técnico, Portugal.

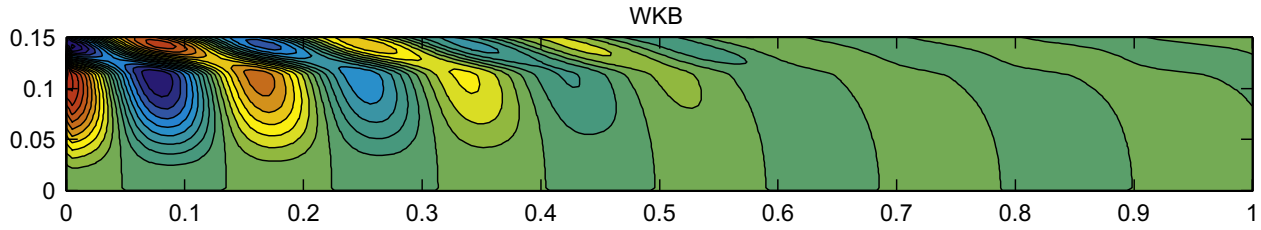

Fig. 18. $\omega = 10$, $m=2$, $n=2$, uniform mean flow velocity $M_0 = 0.3$, strong temperature gradient, $Z(x)$ varies linearly from $1.5-\mathrm{i}$ to $1.5+\mathrm{i}$ ($\mathrm{e}^{-\mathrm{i}\omega t}$ convention).

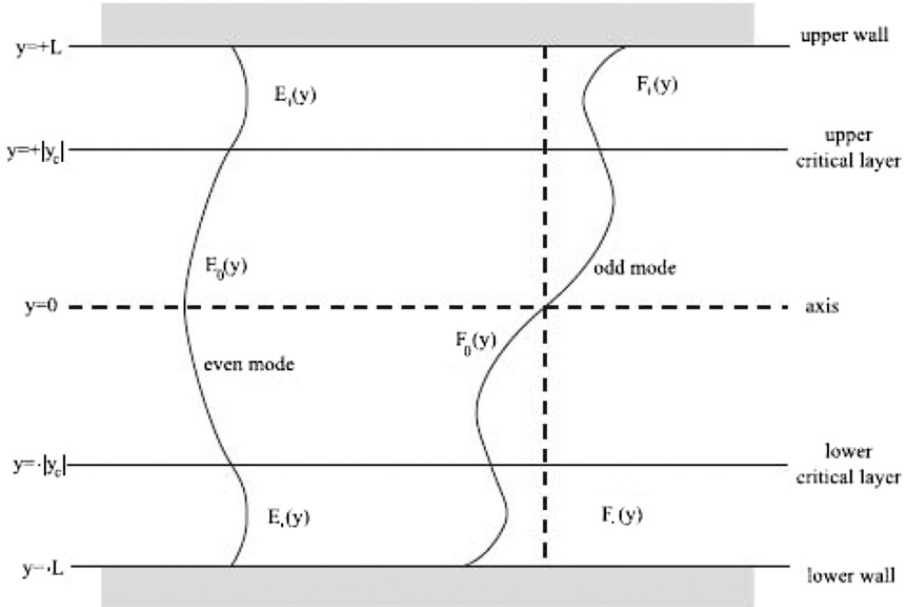

Fig. 19. Conjecture that, if two critical levels are present, there may be a distinct set of eigenvalues and eigenfunctions E, F in three regions: E_0, F_0 between the critical levels $y = \pm|y_c|$, and $E_\pm, F_\pm$ between the critical levels and the walls $y = \pm L$. [Taken from [32].]

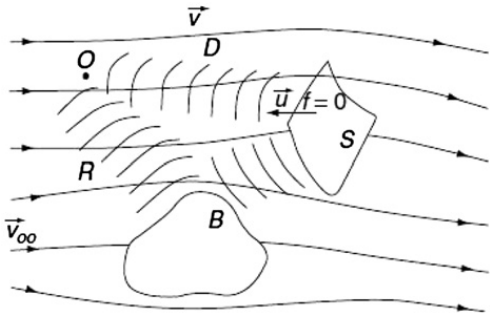

Fig. 20. Observer (O) receiving a direct (D) sound wave from sound source(s) on a surface $f(\vec{x})=0$ moving with arbitrary velocity $\vec{u}$ in a steady, non-uniform, potential mean flow of low Mach number with velocity $\vec{V}(\vec{x})$; the non-uniform flow is due to the introduction in an uniform stream of velocity $\vec{V}_\infty$, of obstacle(s) (B), which also reflect (R) sound waves towards, the observer. [Taken from [37].]

5.8. On sound generation by moving surfaces and convected sources in a flow

The Ffowcs Williams–Hawkings (FW–H) equation has been extensively used to model sound generation by moving surfaces including the noise of aircraft propellers, helicopters rotors and turbomachinery [33]. The FW–H equation allows for surfaces in arbitrary motion in a medium at rest or a uniform flow. The FW–H equation has been extended to: (i) non-uniform mean flow; (ii) other sound sources including vorticity and entropy spots. Concerning (i), in order to exclude vortical and entropy modes, the mean flow is considered to be steady potential, but it may be non-homogeneous and the Mach number is not restricted; likewise for (ii) the sound sources in the flow, that is the forcing of the high-speed wave equation is considered [34]. In the case of non-uniform steady low Mach number mean flow holds a forced convected wave equation [35] whose solution is specified by a generalization of the Kirchhoff integral [36]. A typical situation (Fig. 20) is: (i) the low Mach number incident stream becomes non-uniform due to the presence of bodies (aircraft or helicopter fuselage, compressor cone); (ii) the sound sources are surfaces in arbitrary motion [33] or vorticity or entropy spots [34]; (iii) the sound received by the observer consists of a direct wave plus a scattered wave reflected from the obstacles. All these effects (i)–(iii) are included in the generalized Kirchhoff integral; it differs from the original Kirchhoff integral in replacing the position of the source and observer by a modified position including the unit perturbation potential of the mean flow. This accounts for the scattered wave and also extends the reciprocity principle to the presence of mean flow [37].

Written by L.M.B.C. Campos: luis.campos@ist.utl.pt, Instituto Superior Técnico, Portugal.

5.9. Experimental source characterization techniques for studying the acoustic properties of perforates under high level acoustic excitation

New experimental techniques have been developed for obtaining the acoustic properties of in-duct samples with nonlinear acoustic characteristics [38]. The methods developed are intended both for studies of nonlinear energy transfer to higher harmonics for samples only accessible from one side such as wall treatment in aircraft engine ducts or automotive exhaust systems, and for samples accessible from both sides such as perforates or other top sheets. When harmonic sound waves are incident on the sample nonlinear energy transfer results in sound generation at higher harmonics at the sample (perforate) surface. The idea is that these sources can be characterized using linear system identification techniques similar to one-port or two-port techniques which are traditionally used for obtaining source data for in-duct sources such as IC-engines or fans [39]. The starting point is the so-called polyharmonic distortion modelling [40] which is used for characterization of nonlinear properties of microwave systems. Source models of different complexity were developed and experimentally tested, showing that these techniques can give results which are useful for understanding nonlinear energy transfer to higher harmonics. One example shown in Fig. 21 is the transmission from an incident wave at frequency f on one side of the sample (the B side) to higher harmonics, for a perforate sample with 2% porosity. It can be seen that the reflection is about 5% and the transmission about 2% at a frequency three times the excitation frequency ($3f$). At frequency $5f$ both reflection and transmission coefficients are below 1%.

Written by H. Bodén: hansbod@kth.se, KTH Royal Institute of Technology, Sweden.

5.10. Simulations of duct acoustics with the frequency-domain linearized Navier–Stokes equations

A solver for the frequency-domain linearized Navier–Stokes equations has been developed and applied to model the scattering of sound waves in flow ducts. In [41], the scattering of sound by an in-duct orifice plate (diaphragm) was simulated. Fig. 22 shows density perturbations in the duct and the orifice plate, with both acoustic plane waves and vortical contributions. A power balance equation in the form of the whistling potentiality [42] was calculated to find frequency ranges of amplification and dissipation of impinging acoustic energy, respectively. Amplified frequencies were identified as potential sources of whistling if coinciding with any resonance frequency of the duct system.

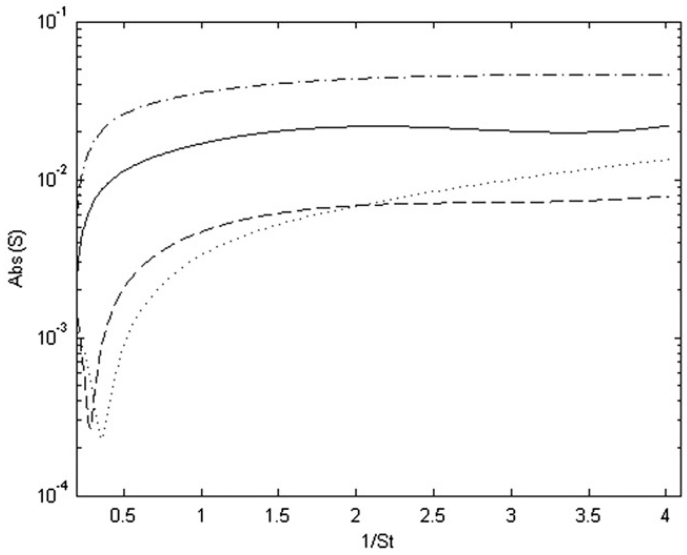

Fig. 21. Absolute value of nonlinear scattering matrix elements: transmission from incident wave at frequency f to transmitted wave at frequency $3f$ (full line); reflection from incident wave at frequency f to reflected wave at frequency $3f$ (dashed-dotted line); transmission from incident wave at frequency f to transmitted wave at frequency $5f$ (dashed line), and, reflection from incident wave at frequency f to reflected wave at frequency $5f$ (dotted line).

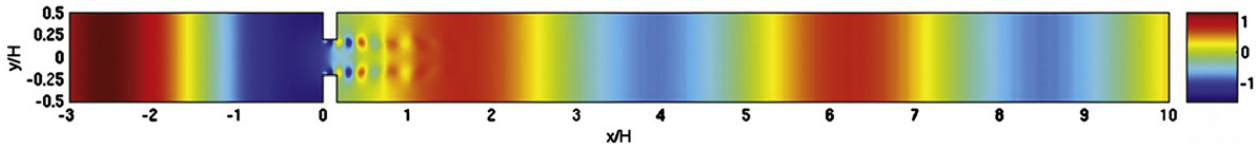

Fig. 22. Real part of the density perturbations in the vicinity of an orifice at a Strouhal number of 0.55. A unit density acoustic plane wave is imposed from the left side and propagates downstream where it is scattered at the orifice, yielding both reflected and transmitted acoustic plane waves as well as vortical structures that are convected downstream by the mean flow.

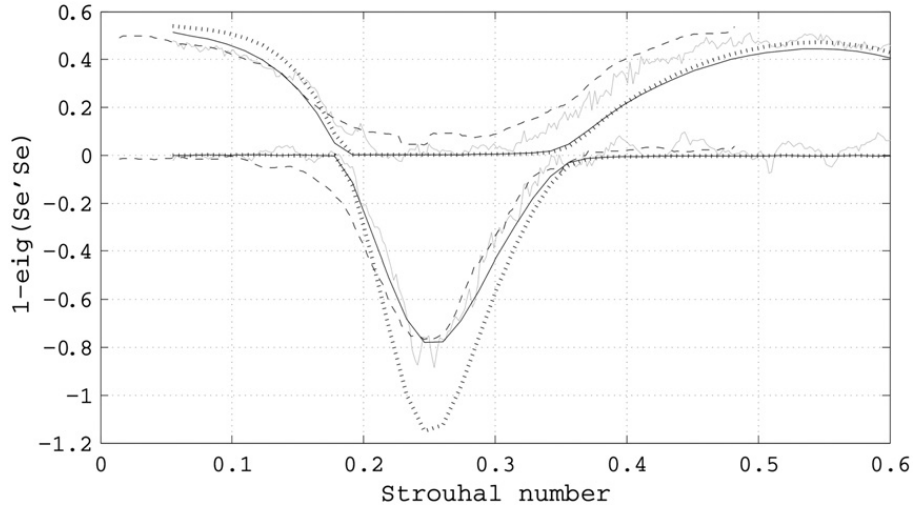

Fig. 23. Power balance of the investigated in-duct orifice plate, as a function of Strouhal number. Values above zero indicate a net dissipation of acoustic energy, and values below zero indicate regions of net production, i.e. possible whistling. Simulations with no-slip boundary conditions (solid black lines); experimental results (dashed lines); simulations with slip boundary conditions (dotted lines); experimental results from [42] (solid gray lines).

Simulations were carried out with and without viscous effects taken into account, and it was shown that the inclusion of viscous acoustic boundary layers were crucial to achieve an accurate level of acoustic amplification, as seen in Fig. 23. This was seen to be due to the vortical–acoustic interaction between the leading and trailing edges of the orifice plate, where the amount of vorticity was exaggerated when slip boundary conditions were imposed on the orifice walls.

The simulated scattering matrix and the reflections from the duct terminations were added to find the response of the entire duct system. When formulated as an eigenvalue system, the Nyquist stability criterion could be used to identify

unstable cases corresponding to whistling systems. Experiments were carried out to validate the simulation results, with good agreement [41].

Written by A. Kierkegaard: axelk@kth.se, KTH Royal Institute of Technology, Sweden.

5.11. Efficient parallel computing with high-order compact schemes for aeroacoustic simulations

An efficient parallel computing methodology for high-order compact finite-difference schemes has been developed by Kim and Sandberg [43]. The new methodology allows implementing compact schemes and filters for aeroacoustic simulations in a massively parallel environment based on domain decomposition and message passing interface (MPI) without generating spurious wave reflections across subdomain boundaries. Conventional parallel computing approaches for compact schemes were limited by low efficiency or the lack of accuracy across subdomain boundaries. The new approach maintains the same level of inter-node communication overhead to that of standard explicit schemes using three halo points, and reduces the level of spurious reflections from subdomain boundaries by two orders of magnitude compared to an earlier work in similar approach [44]. It is shown that, despite the significant improvement, the new methodology may develop some visible reflections in low-speed jet noise simulations where small-scale vortices travel across subdomain boundaries. There is a scope for further work on this issue.

Written by J.W. Kim: j.w.kim@soton.ac.uk and R.D. Sandberg, University of Southampton, United Kingdom.

6. Miscellaneous topics

6.1. Uncertainty quantification for the trailing-edge noise of a controlled-diffusion airfoil

Through an uncertainty quantification (UQ) framework, the uncertainties associated with the prediction of trailing-edge noise have been investigated using RANS or LES computations, in order to determine their respective robustness and accuracy. For this purpose, the two deterministic incompressible flow solvers were coupled with a non-intrusive stochastic collocation method to propagate several aerodynamic uncertainties encountered in a standard trailing-edge noise experiment of a low-speed Controlled-Diffusion (CD) airfoil to predict the far-field noise [45]. The inlet velocity profile is considered as the random variable, reproducing a change of the airfoil angle of attack. Both simulation methods provide the wall-pressure spectra near the airfoil trailing-edge, which are then used in Amiet's acoustic analogy for trailing-edge noise. In the RANS simulations, two different models are used to reconstruct the wall-pressure fluctuations: Rozenberg's deterministic model (YR) [46] directly based on integral boundary-layer parameters, and Panton and Linebarger's statistical model (PL) [47] based on the velocity field in the boundary-layer.

The acoustic results together with experimental measurements are shown in Fig. 24, in terms of mean and 100% uncertainty bars. A good agreement with experiments is found for both methods using RANS information. Larger uncertainty bars are found at high frequencies using the YR model due to the large uncertainties involved in wall shear-stress determination, on which the

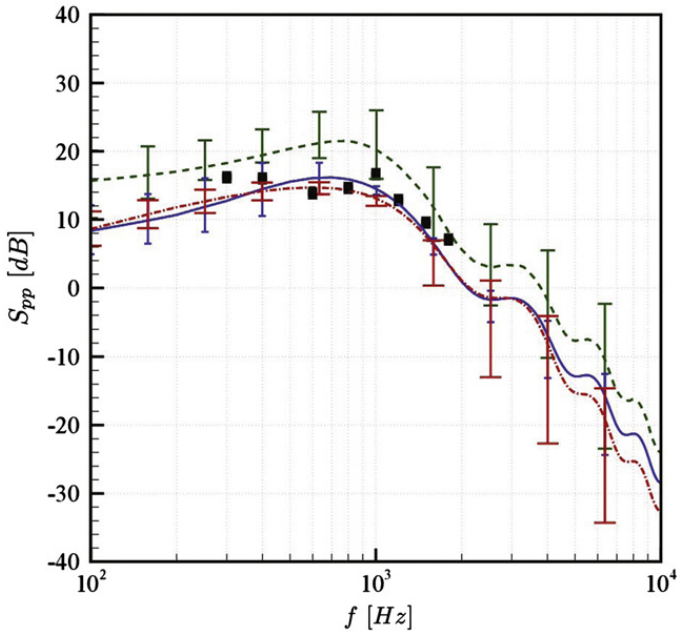

Fig. 24. Mean and uncertainty bars of far-field acoustic spectra in the mid-span plane above the airfoil ($\theta = 90^\circ$) at $R = 2$ m from the trailing edge: YR model (dash-dot and large uncertainty bars); PL model (plain and small uncertainty bars); LES (dash and medium uncertainty bar); experiments (squares).

model is based, at high frequencies. The PL model, not based on the wall shear-stress variable, shows less variation at high frequencies but larger uncertainties at low frequencies caused by the low statistical convergence of the Monte-Carlo integration technique used to integrate the boundary-layer profiles. Finally, due to a different flow behavior encountered in LES computations at lower angles of attack [48], the LES results are shifted to higher levels by about 8 dB. Consequently, the LES uncertainty bars are also found larger than those of the RANS computations.

Written by J. Christophe: julien.christophe@vki.ac.be, von Karman Institute, Belgium, and S. Moreau, Université de Sherbrooke, Canada.

6.2. Acoustic characterization of orifices under grazing flow

The acoustic behavior of orifices in a quiescent medium is relatively well understood since the work of Rayleigh [49]. However, perforated plates are subject to grazing (and possibly bias) mean flows in practical applications such as automotive mufflers or jet engine liners, which significantly affects their acoustic performance. The empirical models derived from numerous experimental studies, as well as those arising from purely analytical approaches, have a limited range of applicability. KU Leuven has developed a numerical methodology [50] in which a Runge–Kutta Discontinuous Galerkin method is used to solve the linearized Navier–Stokes equations, as part of a hybrid approach where the steady, incompressible mean flow is previously obtained from a RANS simulation. A procedure involving a virtual impedance tube and two computations for each case (one with mean flow and one without) makes it possible to isolate the contribution of the mean flow to the orifice impedance. The method has been verified against theoretical models and experimental data from the literature, and is used to study the influence of orifice geometry variations (Fig. 25) on the mean flow contribution to the impedance.

Written by W. De Roeck: wim.deroeck@mech.kuleuven.be, T. Toulorge and W. Desmet, Katholieke Universiteit Leuven, Belgium.

6.3. Aircraft noise modelling and assessment in IESTA

The IESTA (Infrastructure for Evaluating Air Transport Systems) is a platform developed at ONERA (The French Aerospace Lab.) to design and model innovative air transport systems program. The first application of IESTA was dedicated to the environmental impact of the air traffic surrounding airports, including noise and chemical emissions. The acoustics model CARMEN, implemented in IESTA consists of three modules: noise sources, installation effects and atmospheric propagation. The noise source modules for the jet, fan, landing gears and high-lift devices are based on semi-empirical models. They are assessed separately using experimental results from scale models to provide relevant spectral properties and free-field directivity. Installation effects due to the influence of aircraft surfaces on acoustic radiation are included using a ray method. Direct and reflected fields are computed using geometrical acoustics principles, while the diffracted field is approximated using the uniform theory of diffraction. The accuracy of this module is investigated by

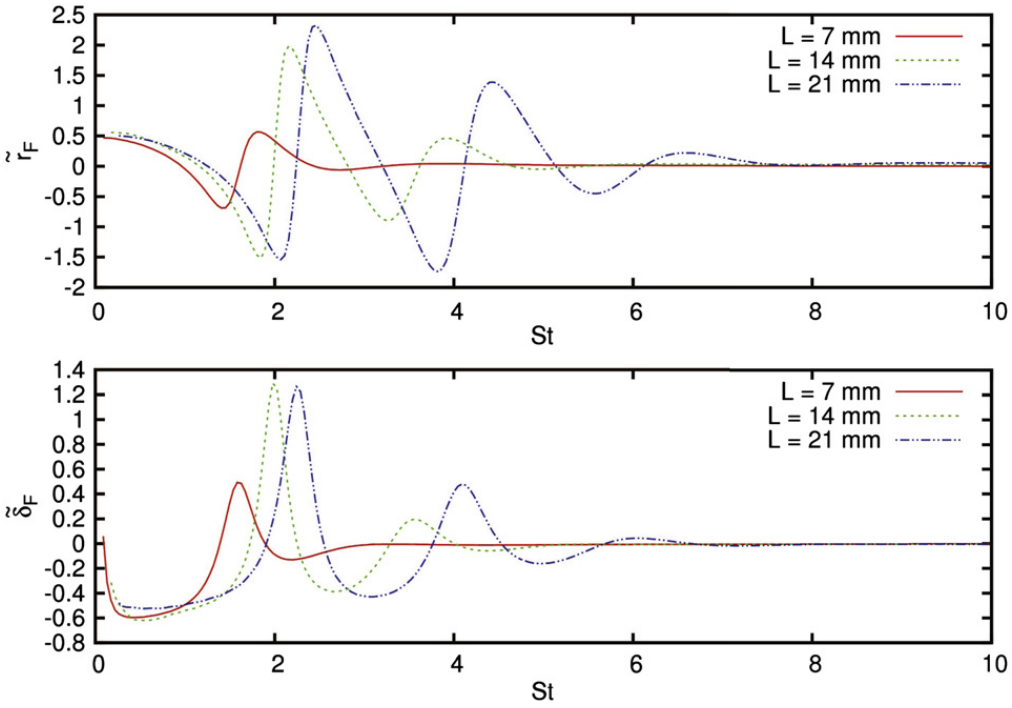

Fig. 25. Scaled contribution of the mean flow to the impedance, as a function of the Strouhal number, for orifices of different lengths.

Fig. 26. AWIATOR: flyover of the A340.

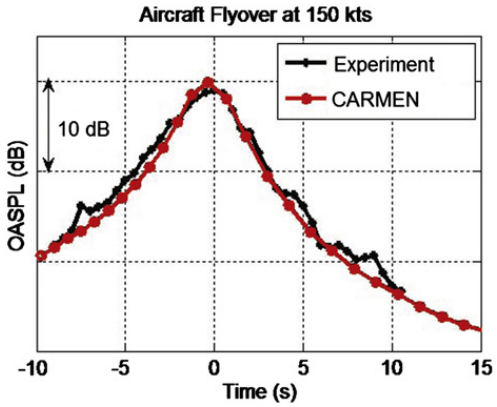

Fig. 27. OASPL during the A340 flyover.

comparison with analytical solutions and BEM computations. The propagation in the non-uniform atmosphere is computed using ray theory, taking into account the wind and temperature profiles and the atmospheric absorption. The CARMEN prediction is assessed against experimental results from an aircraft flyover, performed in the European project AWIATOR (Fig. 26). CARMEN is in very good agreement with the experiment during the whole flyover, where the slat radiation dominates (Fig. 27). ONERA would like to thank Airbus for permitting the use of AWIATOR flight test data [51].

Written by L. Sanders: laurent.sanders@onera.fr, I. Le Griffon and P. Malbéqui, ONERA, France.

6.4. CFD–CAA coupled calculations of a tandem cylinder configuration to assess facility installation effects

Airframe noise is a major source of aircraft annoyance, especially during the approach phase of flight. Within the framework of a NASA–ONERA agreement on airframe noise research, a collaborative study was jointly conducted by ONERA (The French Aerospace Lab.) and NASA Langley Research Center.

The first part of this collaborative effort further improved the coupling between CFD (Computational Fluid Dynamics) and CAA (Computational Aeroacoustics) methods within the framework of a step-by-step aeroacoustic computational tool that uses separate codes to account for the noise generation, propagation, and far-field radiation aspects of an airframe noise problem. More precisely, the so-called 'surface' CFD–CAA coupling approach was assessed and improved by examining a test case including acoustic installation effects. An innovative weak coupling principle was developed [52] that allows the proper handling of the possible acoustic back scatter phenomenon which may be prevalent in installed configurations.

The second part of this study consisted of a numerical assessment of the acoustic installation effects that are inherent to the Quiet Flow Facility (QFF) with respect to the 'tandem cylinders' (TC) experiment. Coupled CFD–CAA computations of the QFF-installed tandem cylinders configuration were conducted [53], relying on the CFD results previously obtained at NASA/LaRC [54]. Taking advantage of the innovative surface weak coupling technique, the coupled calculations (Fig. 28) allowed further validation of the coupling method, as well as an assessment and quantification of the effects on the radiated noise of various devices or features of the Quiet Flow Facility (e.g., mounting side plates, jet collector, nozzle, jet shear layers, etc.).

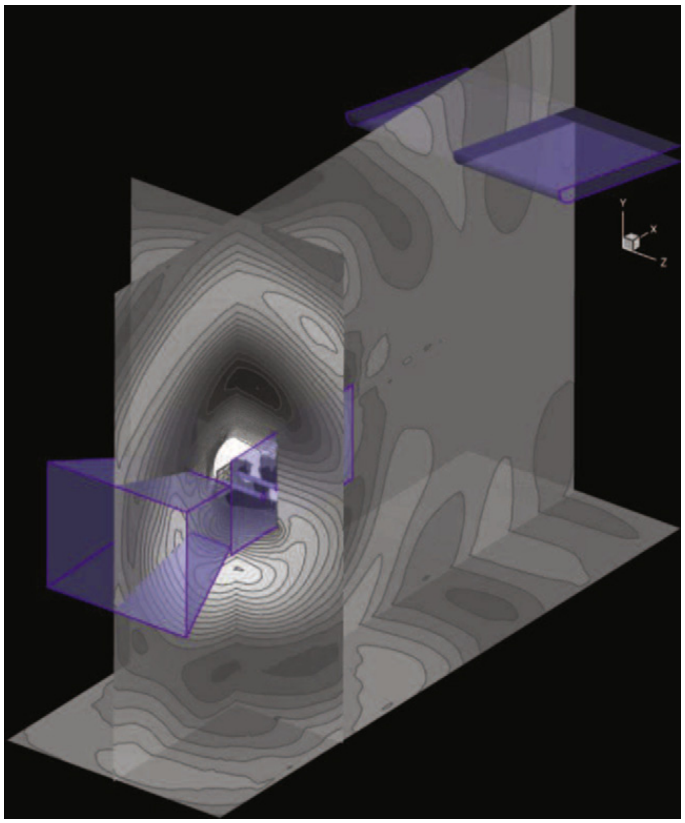

Fig. 28. CFD/CAA coupled calculation of the TC configuration, as installed within QFF facility. CFD computation by NASA/LaRC (CFL3D solver), CAA calculation by ONERA (sAbrinA.v0 code).

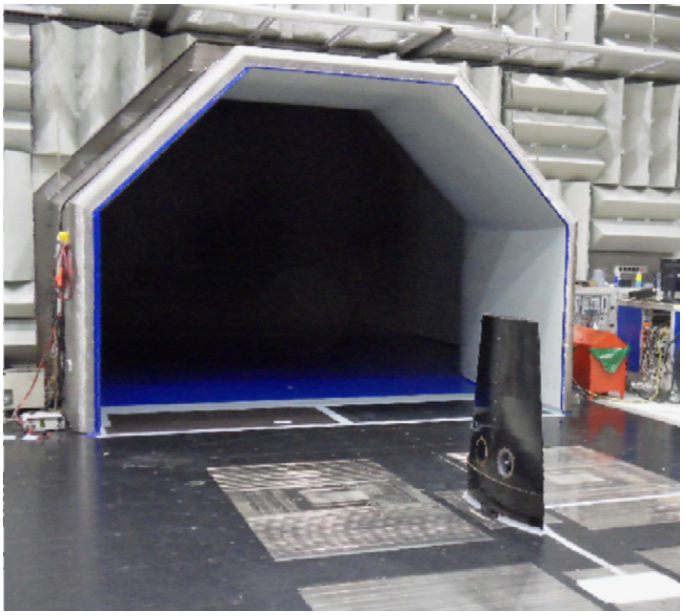

Fig. 29. Fan-in-wing model installed in acoustic wind tunnel.

Written by S. Redonnet: stephane.redonnet@onera.fr, ONERA, France, and D.P. Lockard, M.R. Khorrami and M.M. Choudhari, NASA/LaRC, USA.

6.5. Aeroacoustic investigations of a generic fan-in-wing configuration

A combination of experimental and numerical investigations have been carried out to understand the noise generation mechanisms for a generic fan-in-wing configuration (Fig. 29) which is relevant to vertical and short-take-off and landing (V/STOL) aircraft designs or encapsulated tail rotors. A structured mesh with minimum simplifications has been generated

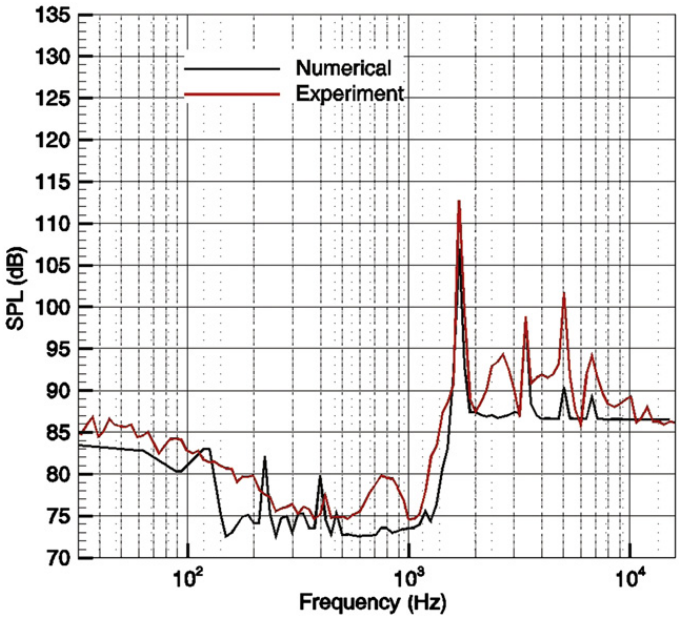

Fig. 30. Predicted sound pressure level compared to measurements on the axis, and $5 \times D$ (diameter) above the fan. (1/12 octave band spectrum).

and a sliding mesh has been used to model the fan rotation. Steady and unsteady Reynolds averaged Navier–Stokes (URANS) computations have been performed using the $k-\omega$ SST turbulence model. The flow physics prediction capability has been assessed against a wide range of aerodynamic measurements in a related work [55–57]. As reference, URANS simulations of the fan installed in a duct with a homogeneous inflow have been conducted.

In the recent analysis, the obtained unsteady flow data was used to determine the radiated sound pressure field by means of the Ffowcs Williams–Hawkings surface integral formulation. The predicted sound pressure level is compared to acoustic measurements at different observer locations. For the first and second blade passing frequencies, a good agreement has been found for all points investigated. The predicted spectrum fairly reproduces the experimental trend (Fig. 30).

Flow separation occurring on the inlet lip induces a considerable inflow distortion thereby causing strong load variations on fan. The overall SPL increases approximately by 10 dB compared to the reference, primarily as the consequence of the distorted inflow. A detailed analysis of the noise sources has been performed.

Written by J. Tirakala: tirakala@aer.mw.tum.de, N. Thouault, J.H. You, C. Breitsamter and N.A. Adams, Technische Universität München, Germany.

References

[1] A. Henning, K. Kaepernick, K. Ehrenfried, L. Koop, A. Dillmann, Investigation of aeroacoustic noise generation by simultaneous particle image velocimetry and microphone measurement, *Experiments in Fluids* 348 (2008) 1073–1085.
[2] A. Henning, L. Koop, K. Ehrenfried, Simultaneous multiplane PIV and microphone array measurements on a rod-airfoil configuration, *AIAA Journal* 48 (2010) 2263–2273.
[3] A. Henning, A. Schroeder, L. Koop, J. Agocs, Causality correlation analysis on a cold jet by means of simultaneous PIV and microphone measurements, *Proceedings of the 16th AIAA/CEAS Aeroacoustics Conference*, AIAA 2010-3753, Stockholm, Sweden, June 7–9, 2010.
[4] L. Bricteux, M. Duponcheel, G. Winckelmans, C. Schram, Jet flow aeroacoustics at $Re=93000$: comparison between experimental results and numerical predictions, *Proceedings of the 17th AIAA/CEAS Aeroacoustics Conference*, AIAA 2011-2792, Portland, Oregon, June 6–8, 2011.
[5] C. Schram, S. Taubitz, J. Anthoine, A. Hirschberg, Theoretical/empirical prediction and measurement of the sound produced by vortex pairing in a low mach number jet, *Journal of Sound and Vibration* 281 (2005) 171–187.
[6] Y. Detandt, G. Degrez, C. Schram, Jet flow aeroacoustics at $Re=14000$: comparison between experimental and numerical simulations, *Proceedings of the 13th AIAA/CEAS Aeroacoustics Conference*, AIAA 2007-3590, Rome, Italy, May 21–23, 2007.
[7] G. Geiser, S. Koh, W. Schroder, Analysis of acoustic source terms of a coaxial helium/air jet, *Proceedings of the 17th AIAA/CEAS Aeroacoustics Conference*, AIAA 2011-2793, Portland, Oregon, June 6–8, 2011.
[8] S. Koh, G. Geiser, W. Schroder, Reformulation of acoustic entropy source terms, *Proceedings of the 17th AIAA/CEAS Aeroacoustics Conference*, AIAA 2011-2927, Portland, Oregon, June 6–8, 2011.
[9] C. Tam, L. Auriault, Jet mixing noise from fine-scale turbulence, *AIAA Journal* 37 (1999) 145–153.
[10] R. Ewert, RPM—the fast random particle-mesh method to realize unsteady turbulent sound sources and velocity fields for CAA applications, *Proceedings of the 13th AIAA/CEAS Aeroacoustics Conference*, AIAA 2007-3506, Rome, Italy, May 21–23, 2007.
[11] R. Ewert, A. Neifeld, A 3-D modal stochastic jet noise source model, *Proceedings of the 17th AIAA/CEAS Aeroacoustics Conference*, AIAA 2011-2887, Portland, Oregon, June 6–8, 2011.
[12] A. Neifeld, R. Ewert, Jet mixing noise from single stream jets using stochastic source modeling, *Proceedings of the 17th AIAA/CEAS Aeroacoustics Conference*, AIAA 2011-2770, Portland, Oregon, June 6–8, 2011.

[13] T. Deconinck, A. Capron, V. Barbieux, C. Hirsch, G. Ghorbaniasl, Sensitivity study on computational parameters for the prediction of noise generated by counter-rotating open rotors, *Proceedings of the 17th AIAA/CEAS Aeroacoustics Conference*, AIAA 2011-2765, Portland, Oregon, June 6–8, 2011.
[14] K. Kucukcoskun, J. Christophe, C. Schram, J. Anthoine, M. Tournour, An extension of Amiet's theory for spanwise-varying incident turbulence and broadband noise scattering using a boundary element method, *Proceedings of the 16th AIAA/CEAS Aeroacoustics Conference*, AIAA 2010-3987, Stockholm, Sweden, June 7–9, 2010.
[15] S. Remmler, J. Christophe, J. Antoine, Computation of wall-pressure spectra from steady flow data for noise prediction, *AIAA Journal* 48 (2010) 1997–2007.
[16] H. Denayer, W. De Roeck, W. Desmet, C. Schram, Extension of Amiet's theory for the aeroacoustic analysis of wing-flap interaction including scattering, *Proceedings of the 18th AIAA/CEAS Aeroacoustics Conference*, AIAA 2012-2096, Colorado Springs, Colorado, June 4–6, 2012.
[17] J. Caradonna, O. Schwartz, P. di Francescantonio, Innovative computational aero-acoustic approach for automotive exhaust systems, *ISMA 2010*, Leuven, Belgium, September 20–22, 2010.
[18] E. Piot, F. Micheli, F. Simon, Optical acoustic pressure measurements in a large-scale test facility with mean flow, *Proceedings of the 16th AIAA/CEAS Aeroacoustics Conference*, AIAA 2010-3752, Stockholm, Sweden, June 7–9, 2010.
[19] T. Ahlefeldt, L. Koop, A. Lauterbach, Aeroacoustic measurements of a scaled half model at high Reynolds numbers, *Proceedings of the 16th AIAA/CEAS Aeroacoustics Conference*, AIAA 2010-3748, Stockholm, Sweden, June 7–9, 2010.
[20] T. Ahlefeldt, L. Koop, Microphone-array measurements in a cryogenic wind tunnel, *AIAA Journal* 48 (2010) 1470–1479.
[21] T. Ahlefeldt, J. Quest, High-Reynolds number aeroacoustic testing under pressurized cryogenic conditions in PETW, *Proceedings of the 50th AIAA Aerospace Science Meeting*, Nashville, TN, AIAA 2012-107, 2012.
[22] C. Spehr, H. Hennings, H. Buchholz, In-flight sound measurements: a first overview, *Proceedings of the 18th AIAA/CEAS Aeroacoustics Conference*, AIAA 2012-2208, Colorado Springs, Colorado, June 4–6, 2012.
[23] S. Haxter, C. Spehr, Two-dimensional evaluation of turbulent boundary layer pressure fluctuations at cruise flight condition. *Proceedings of the 18th AIAA/CEAS Aeroacoustics Conference*, AIAA 2012-2139, Colorado Springs, Colorado, June 4–6, 2012.
[24] G. Corcos, Resolution of pressure in turbulence, *Journal of the Acoustical Society of America* 35 (1963) 192–199.
[25] M. Efimtsov, Characteristics of the field of turbulent pressures at the wall of a boundary layer, *Soviet Physics Acoustics* 28 (1982) 289–292.
[26] D. Gyorgyfalvy, Effect of pressurization on airplane fuselage drag, *Journal of Aircraft* 2 (1965) 531–537.
[27] M. Oppeneer, W. Lazeroms, S. Rienstra, R. Mattheij, P. Sijtsma, Acoustic modes in a duct with slowly varying impedance and non-uniform mean flow and temperature, *Proceedings of the 17th AIAA/CEAS Aeroacoustics Conference*, AIAA 2011-2871, Portland, Oregon, June 6–8, 2011.
[28] M. Goldstein, E. Rice, Effect of shear on duct wall impedance, *Journal of Sound and Vibration* 30 (1973) 79–84.
[29] L. Campos, M. Kobayashi, On the propagation of sound in a high-speed non-isothermal shear flow, *International Journal of Aeroacoustics* 8 (2009) 199–230.
[30] L. Campos, P. Serrao, On the acoustics of an exponential boundary layer, *Philosophical Transactions of the Royal Society A* 356 (1998) 2335–2378.
[31] L. Campos, M. Kobayashi, On the reflection and transmission of sound in a thick shear layer, *Journal of Fluid Mechanics* 424 (2000) 303–326.
[32] L. Campos, J. Oliveira, On the acoustic modes in a duct containing a parabolic shear flow, *Journal of Sound and Vibration* 330 (2011) 1166–1195.
[33] J. Ffowcs Williams, D. Hawkings, Sound generation by turbulence and surfaces in arbitrary motion, *Philosophical Transactions of the Royal Society A* 264 (1969) 321–342.
[34] L. Campos, On 36 forms of the acoustic wave equation in potential flows and inhomogeneous media, *Applied Mechanics Review* 60 (2007) 149–171.
[35] M. Howe, Generation of sound by aerodynamic sources in an homogeneous steady flow, *Journal of Fluid Mechanics* 67 (1975) 597–610.
[36] L. Campos, Emission of sound by an ionized inhomogeneity, *Proceedings of the Royal Society of London A* 359 (1978) 65–91.
[37] L. Campos, F. Lau, On sound generation by moving surfaces and convected sources in a flow, *International Journal of Aeroacoustics* 11 (2012) 103–135.
[38] H. Boden, Experimental source characterization techniques for studying the acoustic properties of perforates under high level acoustic excitation, *Journal of the Acoustical Society of America* 130 (2011) 2639–2647.
[39] H. Boden, M. Abom, Modelling of fluid machines as sources of sound in duct and pipe systems, *Acta Acoustica* 3 (1995) 549–560.
[40] J. Verspecht, D. Root, Polyharmonic distortion modelling, *IEEE Microwave Magazine* (June) (2006) 44–57.
[41] A. Kierkegaard, S. Allam, G. Efraimsson, M. Abom, Simulations of whistling and the whistling potentiality of an in-duct orifice with linear aeroacoustics, *Journal of Sound and Vibration* 331 (2012) 1084–1096.
[42] P. Testud, Y. Auregan, P. Moussou, A. Hirschberg, The whistling potentiality of an orifice in a confined flow using an energetic criterion, *Journal of Sound and Vibration* 325 (2009) 769–780.
[43] J. Kim, R. Sandberg, Efficient parallel computing with a compact finite difference scheme, Computers and Fluids, 58 (2012) 70-87.
[44] T. Sengupta, A. Dipankar, A. Rao, A new compact scheme for parallel computing using domain decomposition, *Journal of Computational Physics* 220 (2007) 654–677.
[45] S. Moreau, D. Neal, Y. Khalighi, M. Wang, G. Iaccarino, Validation of unstructured-mesh LES of the trailing-edge flow and noise of a controlled-diffusion airfoil, *Proceedings of the Summer Program 2006*. Centre for Turbulence Research, Stanford University/NASA Ames, 2006.
[46] Y. Rozenberg, S. Moreau, M. Henner, S. Morris, Fan trailing-edge noise prediction using RANS simulations, *Proceedings of the 16th AIAA/CEAS Aeroacoustics Conference*, AIAA 2010-3720, Stockholm, Sweden, June 7–9, 2010.
[47] R. Panton, J. Linebarger, Wall pressure spectra calculations for equilibrium boundary layers, *Journal of Fluid Mechanics* 65 (1974) 261–287.
[48] J. Christophe, S. Moreau, C. Hamman, J. Witteveen, G. Iaccarino, Uncertainty quantification for the trailing-edge noise of a controlled-diffusion airfoil, *Proceedings of the Summer Program 2010*. Centre for Turbulence Research, Stanford University/NASA Ames, 2010.
[49] J. Rayleigh, *The Theory of Sound*, MacMillan, 1896.
[50] T. Toulorge, Efficient Runge–Kutta Discontinuous Galerkin Methods Applied To Aeroacoustics, Ph.D. Thesis, Katholieke Universiteit Leuven, 2012.
[51] P. Malbéqui, Y. Rozenberg, J. Bulté, Aircraft noise modelling and assessment in the IESTA program, *Proceedings of Inter-Noise*, Osaka, Japan, September 4–7, 2011.
[52] S. Redonnet, On the numerical prediction of aerodynamic noise via a hybrid approach—part 1: CFD/CAA surface coupling methodology, revisited for the prediction of installed airframe noise problem, *Proceedings of the 16th AIAA/CEAS Aeroacoustics Conference*, AIAA 2010-3709, Stockholm, Sweden, June 7–9, 2010.
[53] S. Redonnet, D. Lockard, M. Khorrami, M. Choudhari, CFD–CAA coupled calculations of a tandem cylinder configuration to assess facility installation effects, *Proceedings of the 17th AIAA/CEAS Aeroacoustics Conference*, AIAA 2011-2841, Portland, Oregon, June 6–8, 2011.
[54] D. Lockard, M. Khorrami, M. Choudhari, F. Hutcheson, T. Brooks, Tandem cylinder noise prediction, *Proceedings of the 13th AIAA/CEAS Aeroacoustics Conference*, AIAA 2007-3450, Rome, Italy, May 21–23, 2007.
[55] N. Thouault, C. Breitsamter, N. Adams, Numerical investigation of inlet distortion on a wing-embedded lift fan, *Journal of Propulsion and Power* 27 (2011) 16–28.
[56] N. Thouault, C. Breitsamter, N. Adams, Numerical and experimental analysis of a generic fan-in-wing configuration, *Journal of Aircraft* 46 (2009) 656–666.
[57] N. Thouault, Aerodynamic Investigations on Generic Fan-in-wing Configurations, Ph.D. Thesis, Technische Universitat Munchen, 2010.